Keyblock Stability in Seismically Active Rock Slopes—Snake Path Cliff, Masada

Yossef H. Hatzor, M.ASCE[1]

Abstract: Keyblock stability in the "Snake Path" cliff of the Masada monument, situated on the western margin of the seismically active Dead Sea transform, is studied using field mapping, mechanical analysis, and monitoring of displacement, pressure, temperature, and relative humidity, over a period of 11 months. A linear nonreversible displacement trend is interpreted as the block response to regional microseismicity. A more pronounced cyclic displacement trend however is shown to be a response to climatic changes on the cliff face. This finding introduces a new, time-dependent, failure process in jointed rock slopes—the degradation of shear and/or cohesive strength of joints due climatic effects. Using two-dimensional (2-D) and three-dimensional (3-D) limit equilibrium analyses it is demonstrated that the 2-D solution overestimates the factor of safety against sliding by as much as 15% if water pressures in the boundary joints are considered. Application of a 2-D solution for a truly 3-D case where prismatic blocks are considered proves therefore to not be conservative.

Historical and Geological Background

Scope of Research Program

This research program was triggered by the installation of a new cable car station at the top of the Snake Path cliff in Masada, a project which was completed in late 1999. Several potentially removable keyblocks were identified and mapped above and along the path of a proposed new bridge planned to connect the new cable car station at its anchoring point in the cliff to the formal entrance gate to the monument at the mountain top, a distance of 125 m. Because minute keyblock displacement could place the structural integrity of the proposed bridge at risk, it became necessary to study the stability of the mapped keyblocks, their failure modes, and their actual performance over time, in order to establish adequate support guidelines. In this paper the style of keyblock displacement in a rock cliff is demonstrated, the time dependence is explored, and differences between two-dimensional (2-D) and three-dimensional (3-D) stability analyses are discussed.

Historical Overview

Masada is perhaps the most important national monument in Israel that is visited annually by up to 1 million domestic and international tourists. In order to reach the mountain top tourists can either hike up the Snake Path or take the cable car, the upper station of which is anchored against the steep Snake Path cliff at the mountain top. This isolated mountain, situated in the remote arid Judean Desert of central Israel, was used by the Roman King Herod the Great, between 36 and 30 BC, as an inaccessible fortress in times of political unrest. King Herod built on the mountain top massive fortifications and defense towers, and several grand places, storage facilities and living quarters, fully equipped with dining halls and even steam baths. Large water cisterns were engineered and excavated inside the mountain slopes, and water aqueducts were constructed along the vertical cliffs and they conveyed water from dammed river beds which became filled with floodwater during heavy rain storms. During the revolt against Rome in 70 AD, Masada was the last Jewish stronghold. The Roman army had to lay siege and construct a massive earthen ramp on the western slope of the mountain in order to capture it.

Geological Setting

The Masada mountain is an elongated, geological structure (a horst) that lifts upward and is situated on the western margins of the seismically active Dead Sea rift valley, a distance of up to 10 km from the main fault (Fig. 1). The mountain consists of beds of limestones and dolomites transected by two orthogonal sets of subvertical, closely to widely spaced, open in places, very persistent rock joints, striking NNE and ESE (Fig. 2). Two natural free face attitudes are of concern for rock slope stability analysis of Masada: NNE and ESE striking slopes. Discussion in this paper is restricted to keyblock stability issues in the NNE striking Snake Path cliff which forms the east face of the mountain. In the east the face joint spacing is relatively large (5–10 m), resulting in sizeable keyblocks with total weight ranging between 5 and 15 MN. The locations of three individual keyblocks are shown in Fig. 3. Mapped keyblocks on the east face of the mountain typically rest on eastwardly dipping bedding planes (J1), and are separated from intact rock by one or two "tension cracks" on the back, essentially members of J2 and/or J3.

[1]Dept. of Geological and Environmental Sciences, Ben-Gurion Univ. of the Negev, Beer Sheva 84105, Israel. E-mail: hatzor@bgumail.bgu.ac.il
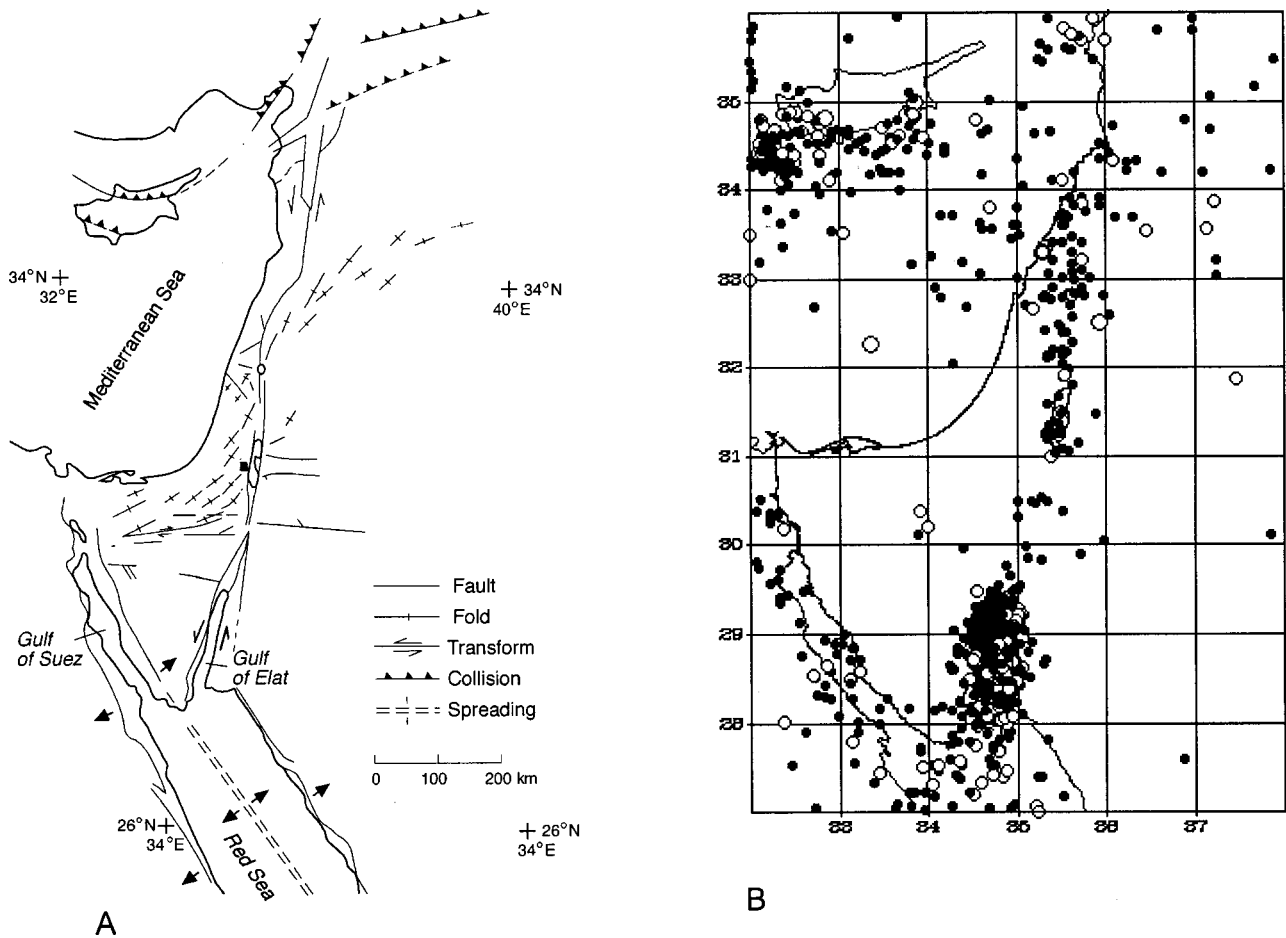
Fig. 1. Geological and seismological setting of Masada. (A) Location of Masada (closed square) with respect to the Dead Sea transform (map after Garfunkel 1981), (B) seismic activity in the Dead Sea rift region between 1950 and present; the location of epicenters is shown by closed circles (data from Geophysical Bulletin of Israel 1996)

Fig. 2. Discontinuity orientation at Masada; bedding planes are J_1 (upper hemisphere projection of poles)

Seismic Hazard at Masada

The Dead Sea transform (Fig. 1) comprises a plate boundary between Africa and Arabia (Garfunkel et al. 1981) and is a segment of the regional Syrian–African Rift System. Along this transform, left lateral strike-slip displacement has taken place since the Middle Miocene (Eyal et al. 1981) at an annual rate of about 5 mm/yr (Garfunkel et al. 1981). Several pull-apart grabens have developed within the rift during its tectonic history, of which the Dead Sea and the Sea of Galilee are two characteristic representatives (Freund 1965; Garfunkel 1981). Recorded seismicity along the Dead Sea rift during the past 50 years is shown in Fig. 1(b). Most of the seismic energy in the region is released along the segments of the fault inside the Gulf of Aqaba (Elat) between Sinai and Arabia.

The Israel Building Code (Code 413) predicts that peak horizontal ground acceleration of 0.2 g is expected along the rift valley with probability of 10% over exposure of 50 years, assuming a damping ratio of 5%. The current code does not make provisions for near field corrections or site effects. The conspicuous topography of the mountain, with a drop of 300 m from the mountain top to the adjacent valley floor across a distance of 600 m, calls for a potential topographic site effect like that found at other rock sites with sharp topographic gradients (see, e.g., Ashford et al. 1997). In order to assess the topography effect at the
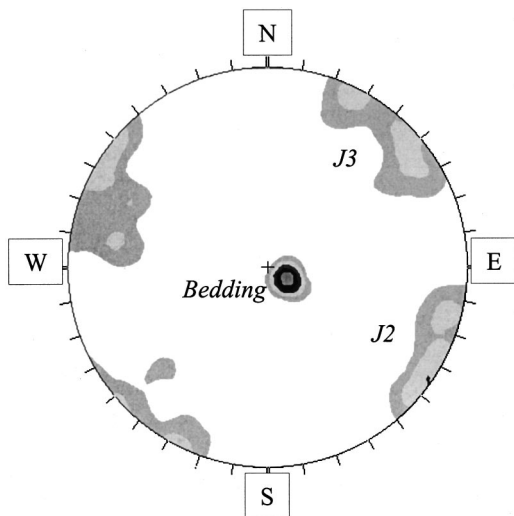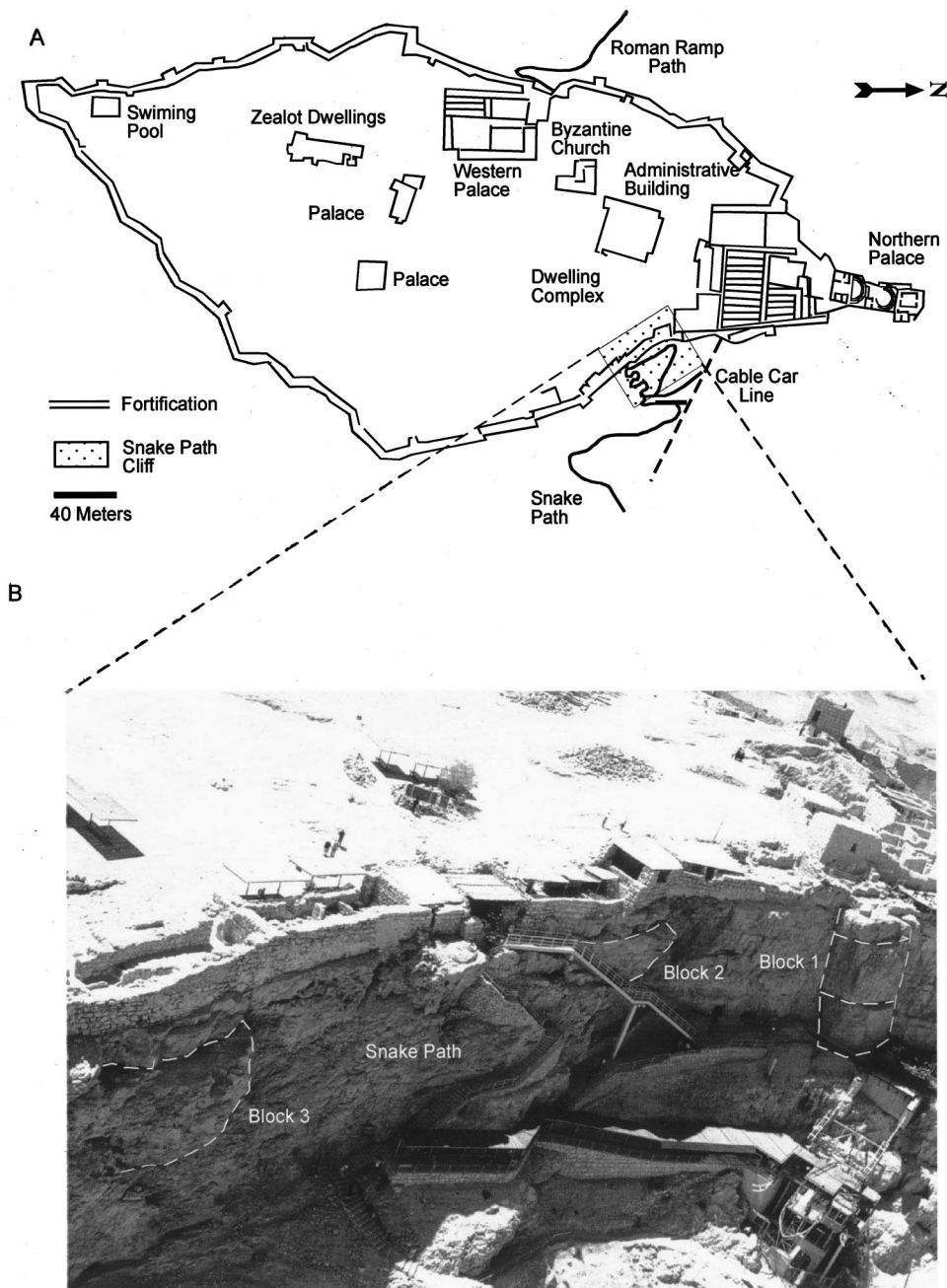
Fig. 3. Snake Path cliff of Masada: (A) Location and (B) three keyblocks studied

site, four seismic stations were deployed in September 10–13, 1998 at the top (stations 1 and 2), midway (station 3), and foot (station 4) of the mountain by Zaslavski et al. (1998). The data recorded consist of several windows of microtremors and one earthquake. Ground motion amplification was determined by three spectral ratio methods: (1) a conventional reference station technique; (2) receiver function estimates based on earthquake data; and (3) the Nakamura method using data of ambient seismic noise. The two bedrock sites (stations 1 and 2), located next to the keyblocks studied at the top of the cliff, exhibited relatively strong spectral amplification for east–west motion, up to a factor of 3.5, with a predominant peak at period 0.71 s. This period is interpreted as the fundamental resonance mode of the site and is attributed to the effect of topography by Zaslavski et al. (1998).

Shear Strength of Sliding Planes

The characteristic keyblock failure mode on the east face involves block sliding along eastwardly dipping bedding planes. The bedding planes at the site are typically wavy to planar, clean and tight in places, but often contain fill material comprised primarily of crushed or reworked dolomite crystals, chalk, and silt [Fig. 4(a)]. In order to assess the angle of friction in dolomite discontinuities, 40 tilt tests were performed, 20 on saw cut planes and 20 on polished planes. The saw cut planes yielded a friction angle of 28° and the polished planes yielded a residual friction angle of 23°. In order to further study the influence of fill material on the angel of friction, an NX size dolomite cylinder was cut diagonally 35° to the axis of the cylinder. The cut was filled with sampled fill
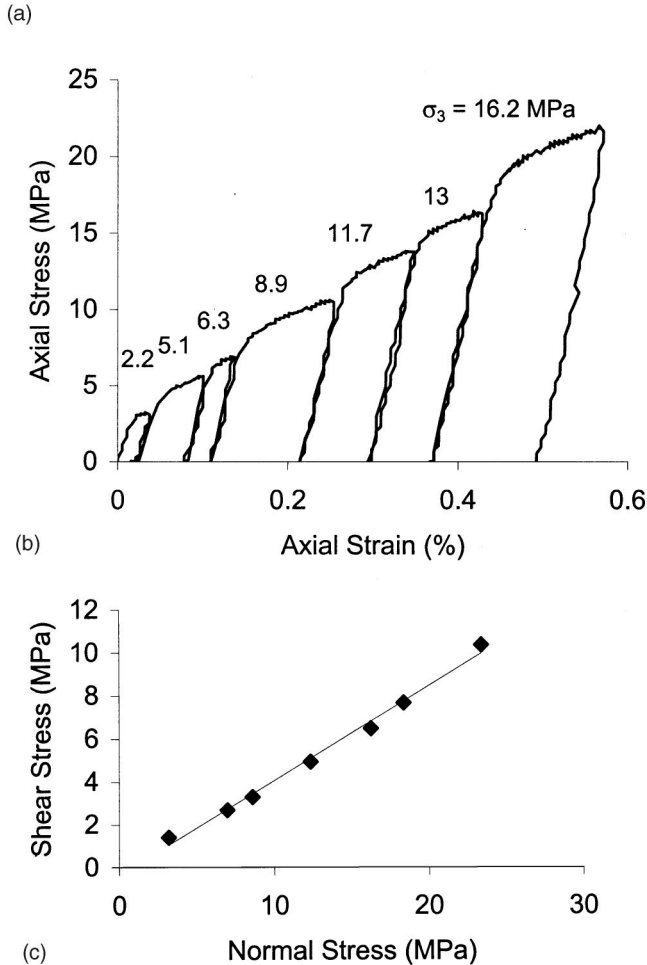
(a)

(b)

(c)

Fig. 4. (a) Example of a filled bedding plane in the Masada dolomite; (b) experimental results of a multisegment triaxial test; (c) failure envelope

material, which was kept at the same water content as that in the field. Triaxial compression was then applied to the filled saw cut under eight different cycles of increasing confining pressure from 0 to 16 MPa. The stress difference was increased until plastic deformation was detected due to the onset of sliding along the filled discontinuity, at which point the axial piston was retracted, the confining pressure increased, and the axial load increased until shearing under a new level of confining pressure commenced [Fig. 4(b)]. The resulting envelope of peak shear and normal stresses indicates a perfectly linear Coulomb–Mohr type

failure criterion with zero cohesion and a friction angle of 22.7° [Fig. 4(c)]. The striking similarity between the results of the segment triaxial test and those of the tilt test of polished surfaces strongly suggests that the residual friction angle is 23°. It should be noted that cohesion was not tested since the specimen contained a precut surface. Cohesion however could play a significant role in the shear resistance of natural sliding planes in the field.

As mentioned earlier, bedding planes in the east face can function as sliding planes for removable blocks. The static factor of safety against sliding along a cohesionless sliding plane is conventionally defined as

$$F.S. = \frac{\tan \phi}{\tan \alpha} \qquad (1)$$

where α=dip angle of the sliding plane. The mean dip of bedding planes, calculated from 25 individual measurements, is 14°. In rock slope stability analysis the mean inclination value of the sliding plane is typically used in support force calculations, and an adequate factor of safety is then applied. In this case a more conservative approach was adopted by choosing a sliding plane inclination of 20°, significantly steeper than the mean (Fig. 2), before a factor of safety was applied. This hidden factor of safety is intended to address the uncertainty associated with the actual inclination of the sliding plane below the removable keyblock. With 20° dip inclination and residual friction angle of 23° the static factor of safety against sliding for dry blocks [Eq. (1)] is as low as 1.17.

Time Dependent Keyblock Displacement

Yield Acceleration of Keyblocks

The preceding discussion suggests that removable keyblocks with a sliding failure mode at the Snake Path cliff are marginally at static equilibrium with an unsatisfactory factor of safety of 1.17. Naturally, such keyblocks are expected to be unsafe under dynamic loading. Goodman and Seed (1966) as well as Newmark (1965) showed that for frictional sliding only, where cohesion along the sliding surface is zero, the down slope, horizontal, yield acceleration for a block resting on a plane with inclination α and friction angel ϕ is given by

$$\alpha_y = \tan(\phi - \alpha) g \qquad (2)$$

where α and ϕ are the plane inclination and friction angle available, respectively. The yield acceleration obtained for sliding keyblocks in the Snake Path cliff is $a_y = 0.05 \ g$, assuming a residual friction angle of 23° and a conservative dip angle of 20°. This is a very low yield acceleration value. By considering empirical attenuation models (e.g., those of Abrahamson and Silva 1997), spectral accelerations greater than 5% g are expected to be triggered by strike-slip events smaller than $M=5$, site periods between 0.1 and 1 s, and rupture distances of up to 10 km. Seismic events of magnitude 3–4.5 are very common at the Dead Sea transform [Fig. 1(b)], and we may therefore conclude that keyblocks with sliding failure modes and low factors of safety would exhibit detectable displacements over time as a response to routine local seismicity.

Monitoring Program

In order to study time dependent keyblock displacements a comprehensive monitoring program was initiated in January 1998 and
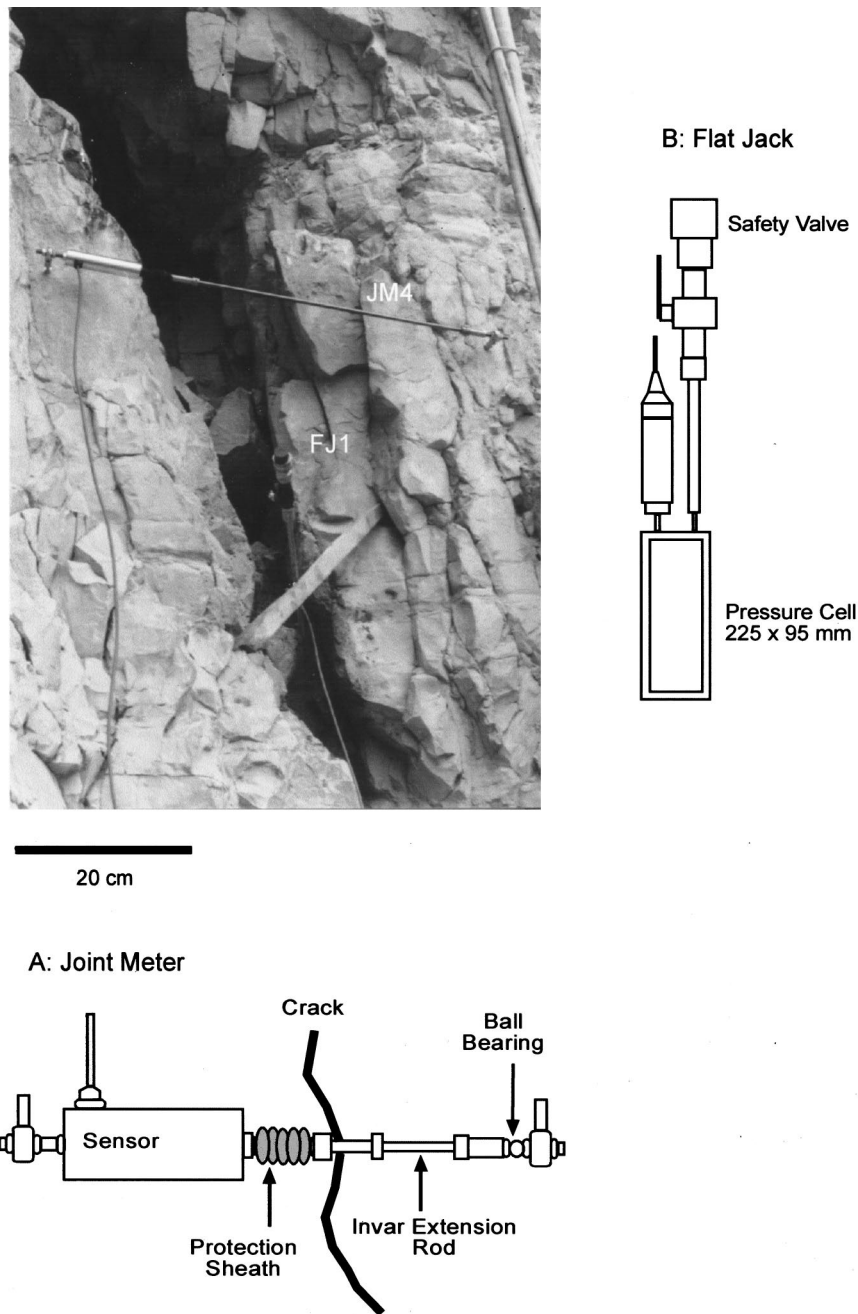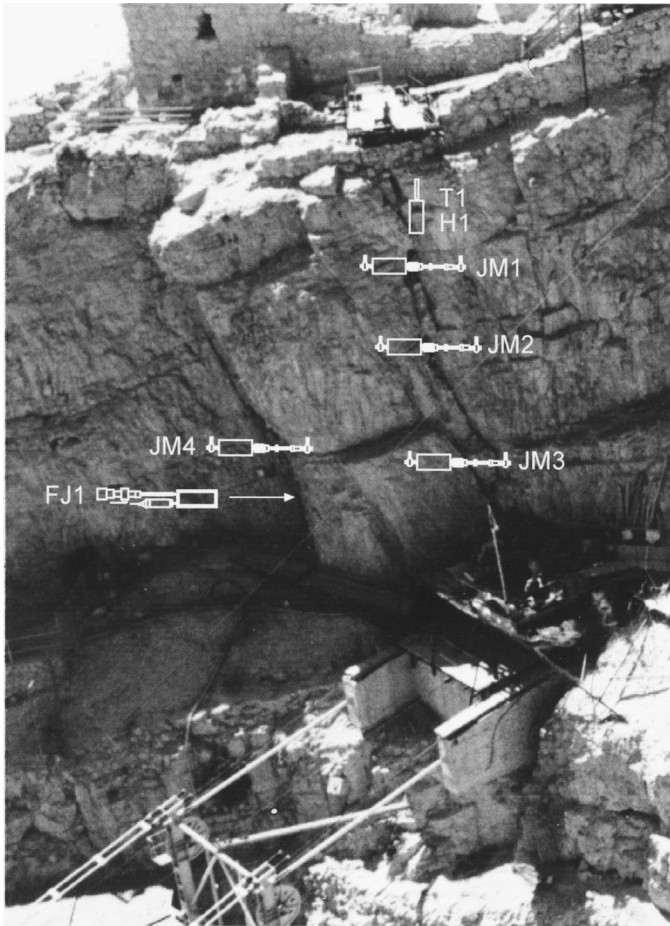
Fig. 5. Joint meter and flat jack installed in block 1: (A) technical drawing of joint meter used in this research; (B) technical drawing of flat jack

continued until November 1998. Three keyblocks were monitored in the Snake Path cliff (Fig. 3) at a data acquisition rate of four to six samples each 24 h. The data collected were stored in a data logger at the site and transmitted to Ben-Gurion Univ. by modem. The monitoring instrumentation consisted of 11 joint meters, 3 flat jacks, 2 relative humidity transducers, and 2 temperature transducers.
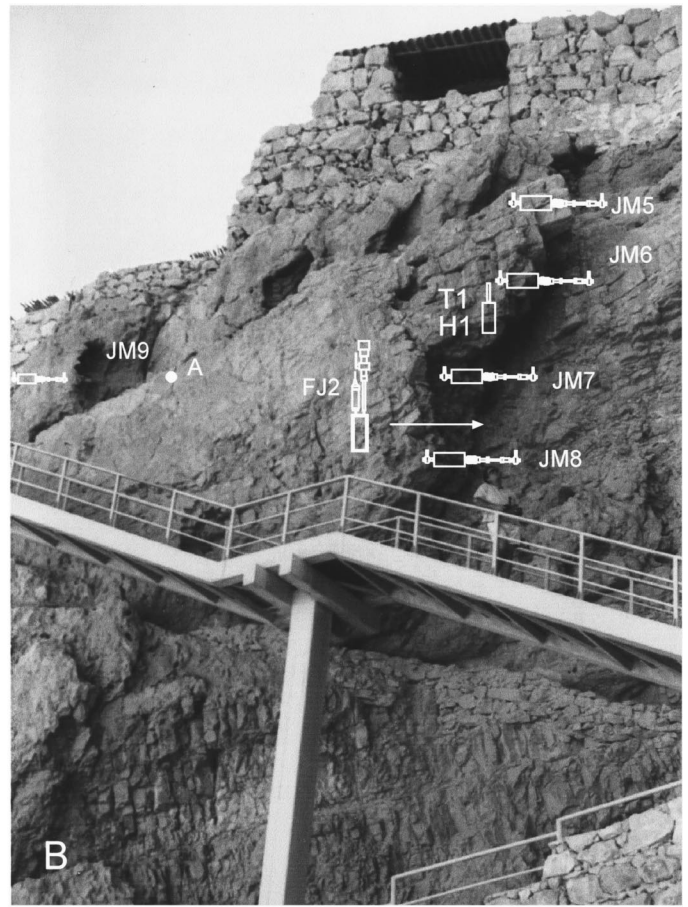
The joint meters (JMs) are LVDTs of 50 mm range (± 25 mm) with 0.5% linearity full scale (model DI800 manufactured by Dina Electronics Ltd.). The calibrated operating range is $-20°$ to $+80°$C. The input voltage is 5 V and the output voltage is typically 100 mV/mm. An example of a joint meter is shown in Fig. 5. The static end of the joint meter contains the LVDT and is anchored to massive rock. An Invar bar (a steel alloy which contains 36% nickel with a thermal expansion coefficient of 1.5 $\times 10^{-6}$ mm/°C) bridges the open joint between static rock and the removable keyblock. The bar is free to displace in any direction; the net displacement is recorded as output voltage, which is translated to engineering units at the data reduction stage. In order to account for thermal effects on the monitoring system, a dummy joint meter of average bar length was installed in a completely intact rock face, near block 2. The output of this joint meter (JM9) over the monitoring period is shown in Fig. 7(b) (bold line). Inspection of JM9 output reveals that thermal effects on the bar are negligible relative to actual block displacements.

The flat jacks (FJs) are thin steel plates with cross-sectional area of 225×95 mm^2 and thickness of 8 mm that are filled with oil (model DI250 manufactured by Dina Electronics Ltd.). The pressure inside the plate is monitored by an electric pressure cell with a pressure range of 20 kg/cm^2 (1,962 kPa), 0.25% linearity

Fig. 6. Monitoring device location (A) in block 1 and (B) in block 2 (JM=joint meter, FJ=flat jack, H=relative humidity transducer, T=temperature transducer)
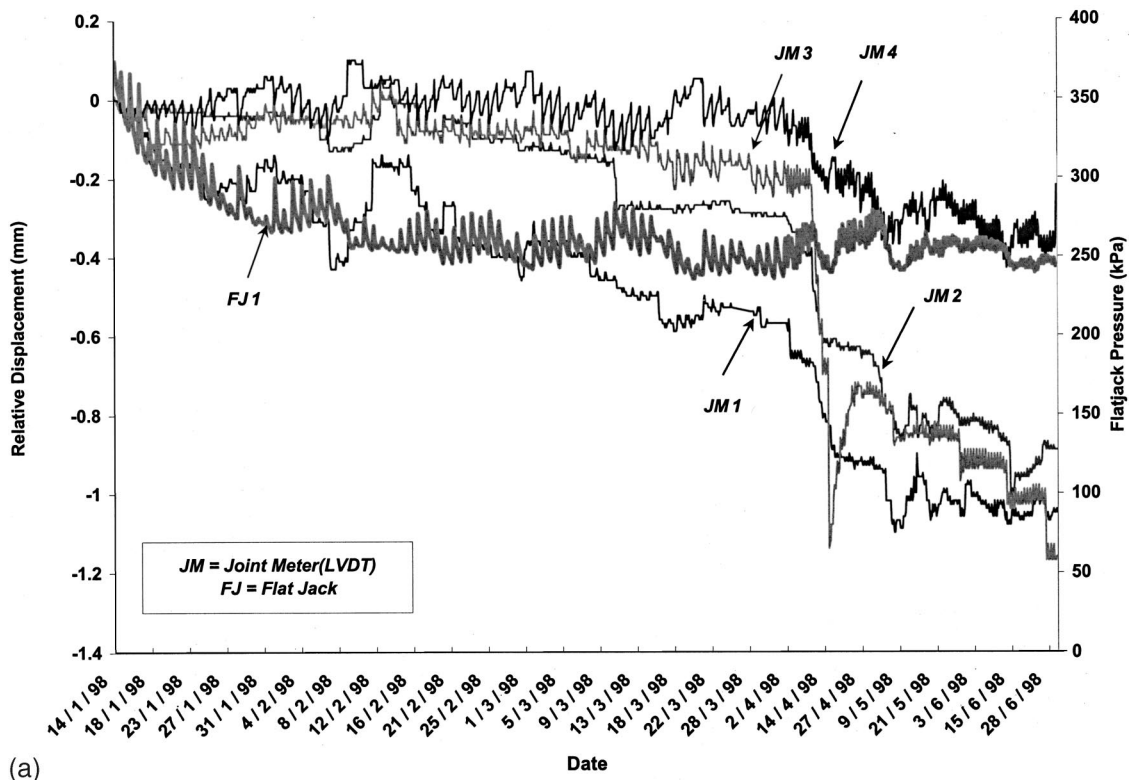
full scale, and temperature operating range of −20 to +80°C (model DI260 manufactured by Dina Electronics Ltd.). The flat jacks were placed at the toe of each removable block using cement to fill the gaps between the plate and the joint in which they were placed. The flat jacks were inflated to initial pressures of between 100 and 300 kPa, but the initial pressures decreased over the monitoring period due to setting of the cement. Once the flat jacks were positioned, any motion of the keyblock was immediately detected by an instantaneous change in pressure. The flat jack pressures recorded were influenced by day/night temperature fluctuations, but the amplitude of these changes in pressure was much smaller than changes in pressure due to actual block displacement (see Fig. 7).

Relative humidity (RH) and platinum thermo-resistance meters (T) were placed in blocks 1 and 2 inside or near the "tension crack" at the back of the block. A relative humidity range of 2–98% could be recorded by the RH transducers (model DI107, Dina Electronics Ltd.), with 1% linearity full scale and operating temperature range of −20/+60°C. A temperature range of −25 to +105°C could be recorded by the thermoresistance meters (T) transducers with 0.15°C linearity full scale (model DI106, Dina Electronics Ltd.).
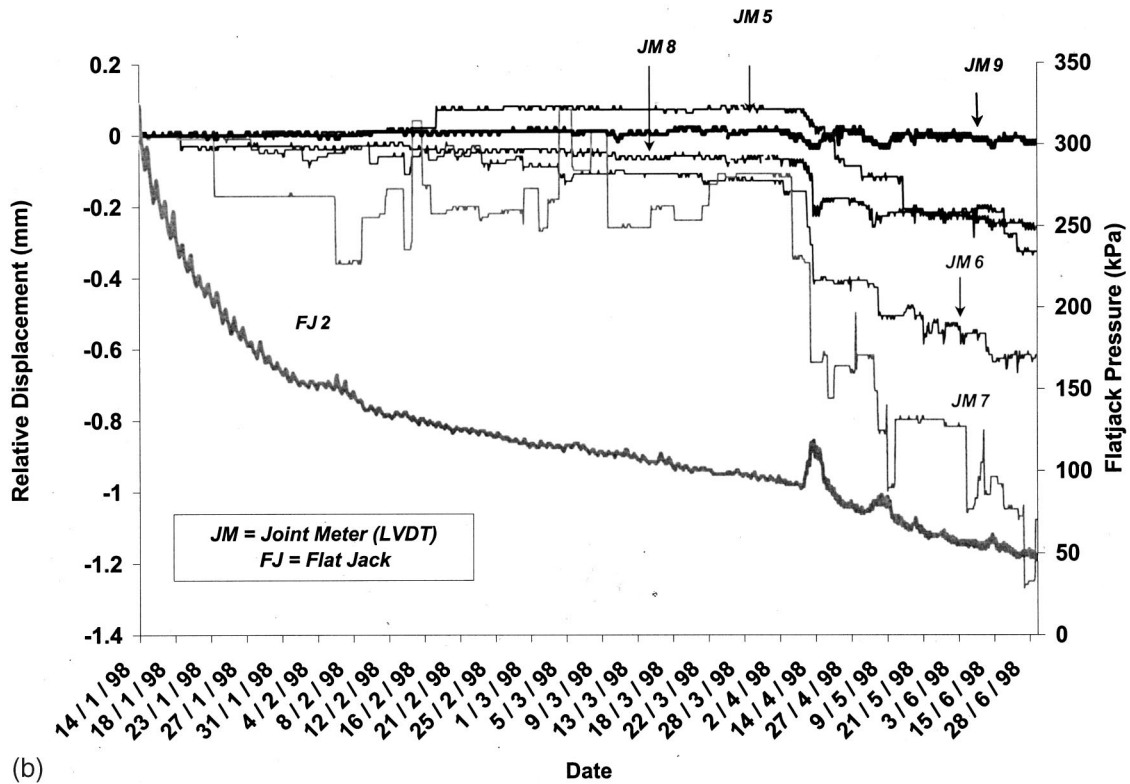
Monitored Keyblocks

Block 1 is a 13.7 MN (1,400 ton) prismatic block rested on an easterly dipped (J1) bedding plane and separated from the cliff by two orthogonal J2 and J3 tension cracks (Fig. 2). The block height is 15 m and its width is about 10 m. Block 1 rests directly above the old cable car station (Fig. 3) and is situated along the path of the proposed bridge to connect the new cable car station to the monument entrance gate at the mountain top. The block has clearly separated from the cliff over geologic and historic times by accumulated displacement of up to 20 cm (see the span of the joint meter in Fig. 5). Four joint meters were mounted between the block and the cliff across the open tension cracks at the back of the block (JM1–4), one flat jack (FJ1) was mounted at the lower part of the block, and one relative humidity (RH1) and one temperature (T1) transducer were mounted inside an open tension crack at the back of the block [Fig. 6(a)].

Block 2 is a rock block separated from the cliff on one end by a wide open joint [see Fig. 6(b)]. This block contains a tensile fracture which extends from point A in Fig. 6(b), vertically downwards, The weight of the block may induce growth and propagation of this crack which, if not arrested, could eventually isolate

Fig. 7. Block displacement output between January 14 and June 30, 1998; JM=joint meter (mm), FJ=flat jack (kPa); (A) block 1, (B) block 2, (C) block 3
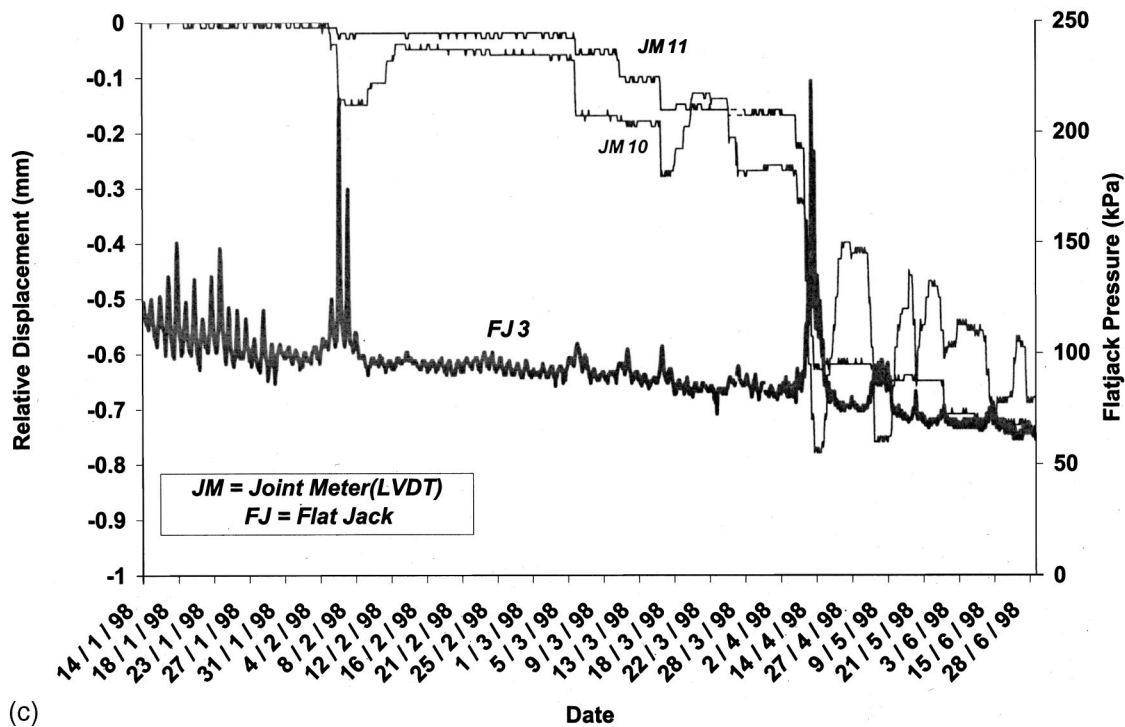
Fig. 7. (*Continued*)

the block from the rock mass. Four joint meters (JM5–8) were installed across the open joint, one flat jack (FJ2) was installed at the base of the block, and one relative humidity (RH2) and one temperature (T2) transducer were installed within the open fracture. The response of the intact cliff was monitored by JM9, which was mounted on solid rock, near block 2.

Block 3 is monitored for long-term observation of block displacement. JM10 and JM11 were mounted across the tension crack at the back of the block, and FJ3 was mounted at its base.

Cable bolt support for blocks 1 and 2 was installed between July and August 1998 and therefore natural displacements could be monitored in these blocks for a 6-month period only, from January to June 1998. The monitoring output of unsupported block 3 provided a continuous annual record of displacement from January to November 1998.

Results of the Monitoring Program

Three continuous records of keyblock displacement from January 14 until June 30 are shown in Fig. 7. Joint meter displacement (in mm) and flat jack compression (in kPa) are plotted as a function of time. A total block displacement of up to 0.3 mm during the first 3 months of monitoring was detected in the three blocks, amounting to a displacement rate of 0.003 mm/day, or 1.2 mm/yr. This displacement rate could manifest block response to local microseismicity. An abrupt displacement episode was detected in mid-April 1998 when the three blocks exhibited displacement of up to 0.8 mm over a period of 3 days (Fig. 8). The bedrock remained static during the entire monitoring period [JM9 is shown in bold face in Fig. 7(b)]. The abrupt displacement event, detected in the three blocks was coupled with a pulse of flat jack compression, as would be expected due to their being installed at the base of each block [see Figs. 7(b and c)]. Superimposition of three representative joint meter outputs from three blocks (JM3 from block 1, JM6 from block 2, and JM10 from block 3) as well

as the bedrock output (JM9) over the same time and displacement scales is shown in Fig. 8. The contrast between the slower displacement rate between January and April and the abrupt displacement episode in mid-April is clearly evident in Fig. 8.

Analysis of Keyblock Displacement Output

The proximity of the Snake Path cliff to the Dead Sea transform suggests that the displacement episode in mid-April could be a response to strong ground motion due to earthquakes in the rift. Two seismic events were recorded during the same period by the seismic network of the Geophysical Institute of Israel (GII): $M = 4.4$ and 4.3 strike-slip events in the Gulf of Elat (Aqaba) between April 7 and April 10, with the epicenter greater than 250 km from the site. These were the only major seismic events recorded in the region 2 months prior to until 1 month after mid-April. Considering the modern attenuation relationships between peak horizontal ground acceleration and horizontal distance from the epicenter (see, e.g., Abrahamson and Sheldock 1997), a magnitude 4.5 earthquake would have had to occur at a distance not greater than 20 km from the site to generate the required 5% g peak ground acceleration at the Snake Path cliff. While the detected slower displacement rate of 0.003 mm/day over a period of 4 months could represent block response to local seismicity, it seems unlikely that the abrupt 0.8 mm displacement represents keyblock response to the remote earthquake registered by the GII.

An alternative cause of block movement could be temperature and humidity effects. In Fig. 9 temperature (T2) and relative humidity data (RH2) measured at block 2 are superimposed on displacement readings from block 3 for the entire duration of the monitoring program, January to November 1998. The temperature and relative humidity outputs measured at block 1 are essentially identical to those measured at block 2, both of which represent the climate within the open tension cracks at the cliff studied. Therefore, superimposition of climatic measurements from block
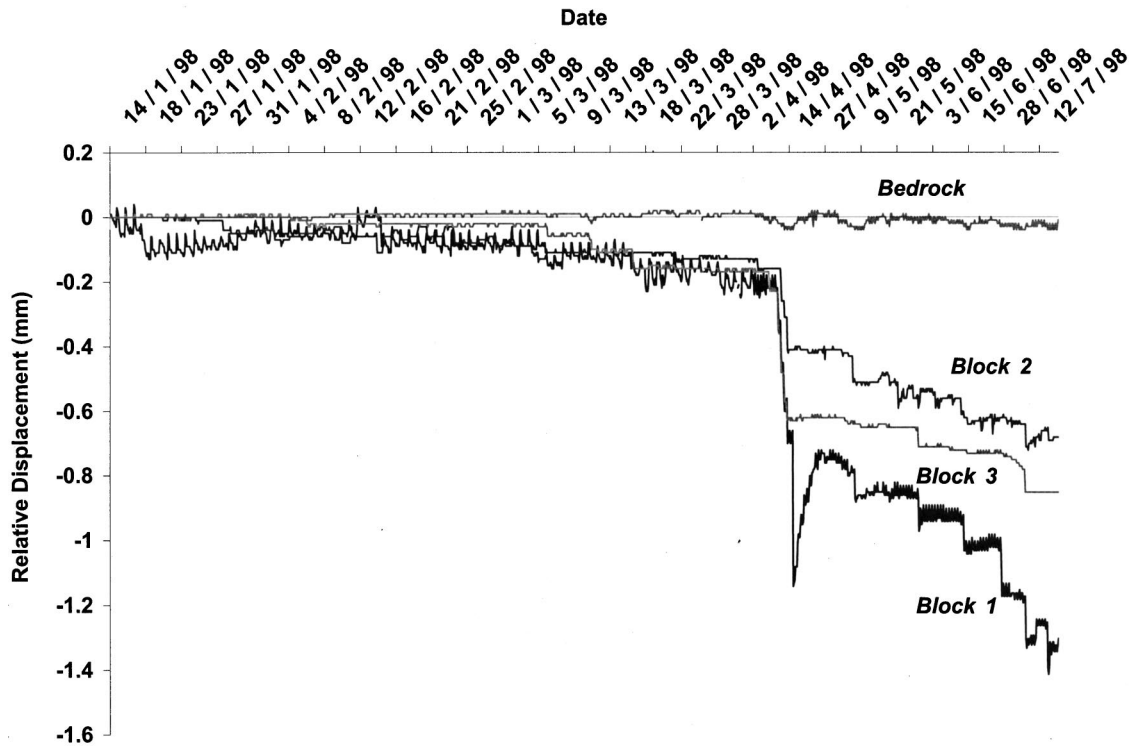
Fig. 8. Bedrock output (JM9) and one representative joint meter output from each keyblock from January to July 1998; note large displacement episode in mid-April
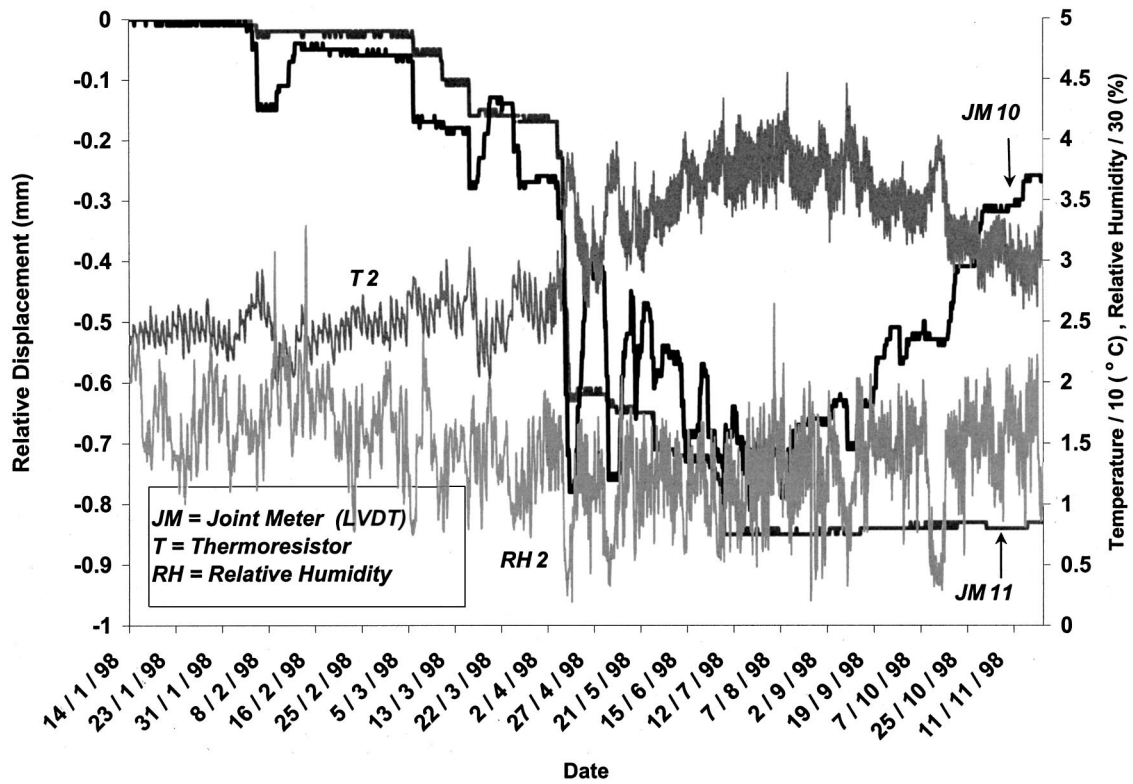

Fig. 9. Output of temperature and relative humidity transducers superimposed on displacement output for block 3 over 11-month period; T2/10: temperature data measured at block 2 divided by 10; RH2/30: relative humidity data measured at block 2 divided by 30
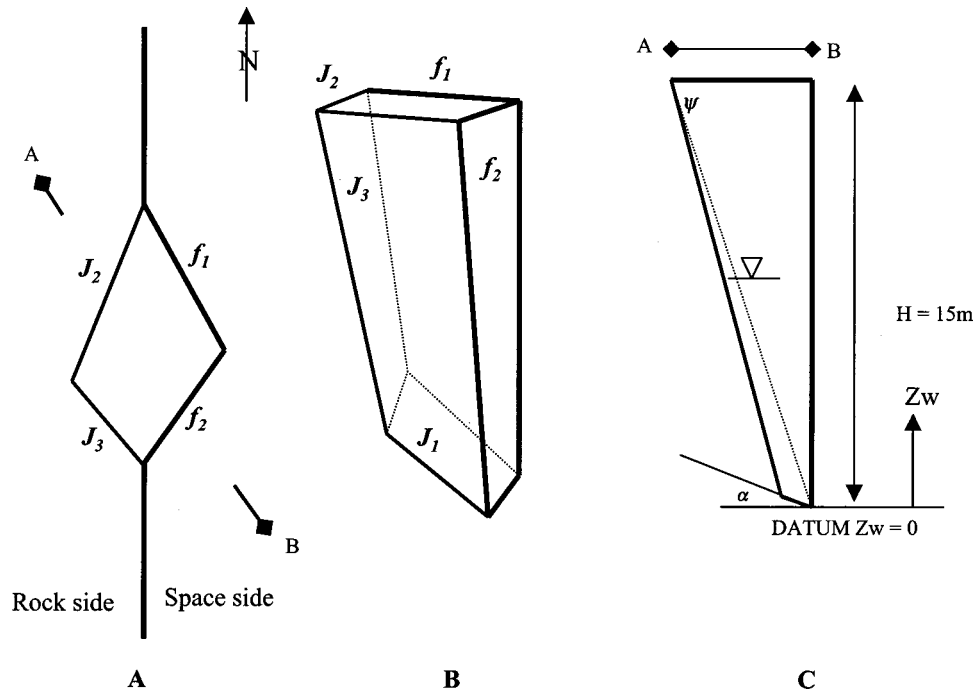
Fig. 10. Geometry of block 1: (A) plan view, (B) three-dimensional view, (C) cross section (f denotes free surface, j denotes joint plane, α the true dip of the bedding plane$=20°$, ψ the apparent dip of J_2 in cross section$=76°$; water table in saturated case shown by dashed line in cross section.

2 on displacement output data of block 3, for which measurements were not performed, is justified. An increase in temperature from 25 to 35°C was detected between April 9 and April 11. This warming event is also expressed by a decrease in humidity from 50 to 13% over the same 3-day period. The dates of the climatic fluctuation match the data of the large displacement event detected in all blocks monitored, suggesting that the cause of the event is climatic. Furthermore, the displacement output in block 3 is cyclical (Fig. 9) and most of the deformation is recovered by the end of November (see the output of JM11). The apparent permanent displacement exhibited by JM10 is attributed to the direction in which it was installed, thus prohibiting detection of reverse motion; all other LVTDs were mounted subhorizontally, thus allowing sensitive detection of reverse motion.

It may be concluded that climatic warming and not seismic ground motion triggered the large displacement episode of mid-April. The slower, linear, rate of opening between January and April could be attributed either to climatic effects or to local microseismicity. In either case the great sensitivity of the blocks attests to their marginal degree of stability. Furthermore, large wavelength cyclic deformations like those exhibited by block 3 between April and November could gradually degrade the shear strength of the sliding planes, as well as the cohesive bond (where it exists) across the tension cracks.

Static and Pseudo-Static Limit Equilibrium Analyses

Blocks 1, 2, and 3 were mapped and monitored at the Snake Path cliff (Fig. 3). Blocks 2 and 3 are not fully isolated from the rock mass and their failure must involve growth and propagation of partially developed tension cracks at the back. Block 1, the largest and most dangerous in the Snake Path cliff, is finite and removable from the rock mass. Block 1 is used here to discuss and

demonstrate several important issues concerning stability analysis of keyblocks in rock slopes. The analysis is limited to sliding along pre-existing discontinuities. Block failure due to joint propagation and fracture of intact rock is not considered here.

Rotation Versus Sliding Analysis: 2-D Approach

The geometry of block 1 is illustrated in Fig. 10. The composite tension crack (formed by the intersection of J_2 and J_3) and free face (formed by the intersection of f_1 and f_2, members of principal joint sets 3 and 2, respectively) are evident in the plan and three-dimensional views [Figs. 10(A and B)]. The tall slender shape of the block is evident in the cross section [Fig. 10(C)].

Block 1 is safe under static loads against forward rotation around the toe, as long as the joints remain dry, because its weight vector is directed towards the rock. Two-dimensional forward rotation analysis reveals that a water head of at least 6 m inside the tension crack would be required to rotate the block about its toe. Two-dimensional sliding analysis for an increase in the water head in the tension crack indicates that a water head of less than 1 m would be sufficient to initiate sliding. Sliding rather than forward rotation is therefore expected to be the governing failure mode under saturated conditions. The following three-dimensional analysis is based on the assumption of a sliding failure mode for block 1.

Three-Dimensional Sliding Analysis: Completely Saturated Case

A graphical solution for a three-dimensional, static, limit equilibrium analysis with joint water forces for block 1 is shown in Fig. 11. Hatzor and Goodman (1997) reviewed the essentials of the graphic solution method, originally proposed by Londe et al. (1970). The solution procedure involves the concept of a friction
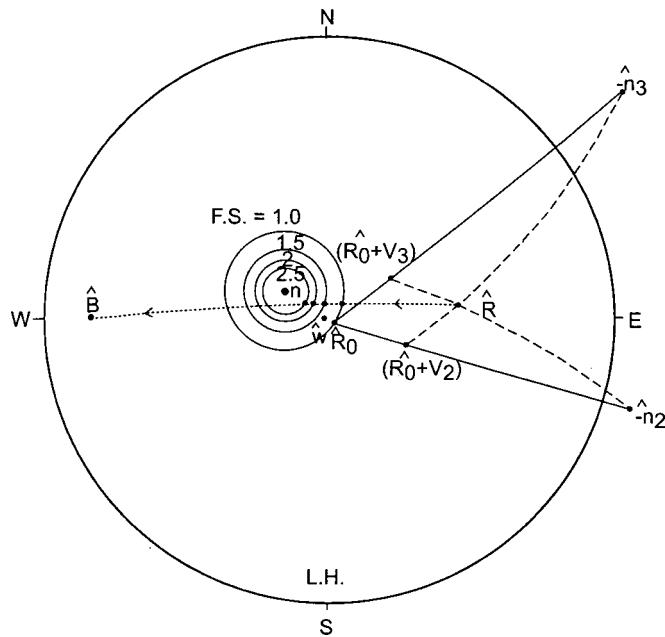
Fig. 11. Graphical solution for a static, fully saturated, three-dimensional, limit equilibrium analysis of block 1 (lower hemisphere projection); B is the total support force

circle, or friction cone (Talobre 1967; Goodman 1976). It should be recalled that stereographic projection is only used to plot the direction of unit vectors and to measure angles between vectors along their common planes. The magnitude of the vectors plotted must be obtained using standard vector techniques. The following forces are considered: $\mathbf{W}$–The block weight, plots at the center of the reference circle in lower hemisphere stereographic projection; $\mathbf{U}$–The resultant water force which acts on the base plane (J_1); this water force acts in the direction parallel to the inward normal of J_1, denoted $-\mathbf{n_1}$ (the outward normal direction with respect to the block is considered positive); $\mathbf{V_2}$–The resultant water force that acts on J_2 in direction $-\mathbf{n_2}$; $\mathbf{V_3}$–The resultant water force that acts on J_3 in direction $-\mathbf{n_3}$; $\mathbf{R}$–The active resultant, the sum of the four forces above.

The resultant water forces in the joints are found by assuming that the tension cracks (J_2 and J_3) and the sliding plane (J_1) are completely submerged under a convex water table surface, which coincides with the top of the block at the lines of intersection between J_2 and J_3 and the horizontal plane [at level $z=15$ m in Fig. 10(C)], and which meets the atmosphere at the bottom of the block (at level $z=0$ m). These assumptions may apply in the case of a heavy rainstorm during which the joints become saturated for a short duration of time. The water force which acts on a submerged surface i is given by the product of water pressure at the centroid of the surface p_{ci}, and the submerged surface area A_i:

$$v_i = p_{ci} A_i = \gamma_w h_{ci} A_i \qquad (3)$$

where h_{ci}=water head at the centroid of the surface (Mironer 1979). The exact block dimensions and force magnitudes pertinent to the analysis are provided in Table 1.

Support Calculations

In order to stabilize the active resultant ($\mathbf{R}$) it must be shifted, by application of a support force ($\mathbf{B}$), into one of the friction circles drawn about the outward normal of the sliding plane ($\mathbf{n_1}$) in Fig.

Table 1. Input Parameters for 3-D Limit Equilibrium Analysis of Block 1

Bedding plane orientation (J_1)	20/124 (dip/dip direction)
Tension crack orientation (J_2)	84/107
Tension crack orientation (J_3)	75/052
Free surface orientation (f_1)	84/060
Free surface orientation (f_2)	90/136
Unit weight of rock (γ)	25 kN/m^3
Cohesion of sliding plane (c)	0
Angle of friction of sliding plane (ϕ)	20°
Block height	15 m
Block volume	563 m^3
Block weight ($\mathbf{W}$)	14,075 kN
Area of J_2	106 m^2
Water head above centroid at full saturation ($h_{c,2}$)	6.5 m
Area of J_3	92.4 m^2
Water head above centroid at full saturation ($h_{c,3}$)	6.5 m
Area J_1	28 m^2
Water head above centroid at full saturation ($h_{c,1}$)	5.5 m
Assumed total water force on J_2 at full saturation ($\mathbf{V_2}$)	6,759 kN
Assumed total water force on J_3 at full saturation ($\mathbf{V_3}$)	5,866 kN
Assumed total water force on J_1 ($\mathbf{U_1}$)	1.511 kN

Note: See the text and Fig. 10.

11. The angle between the normal and the F.S.=1.0 circle is the available angle of friction, in this case 23°. The friction circles that correspond to F.S.=1.5, 2.0, and 2.5 are found by repeated application of Eq. (1).

When water pressures in the base plane are considered, the resultant $\mathbf{Ro}=\mathbf{W}+\mathbf{U}$ plots on the friction circle corresponding to a safety factor of 1.0, namely, the block attains limiting equilibrium. In order to find the active resultant under water force contributions from both J_2 ($\mathbf{V_2}$) and J_3 ($\mathbf{V_3}$), in addition to the base plane water force $\mathbf{U}$, the following vector operation is performed using the stenographic projection:

$$(\mathbf{W}+\mathbf{U})+\mathbf{V_3}+\mathbf{V_2}=(\mathbf{Ro}+\mathbf{V_3})+\mathbf{V_2}=(\mathbf{Ro}+\mathbf{V_2})+\mathbf{V_3}=\mathbf{R} \quad (4)$$

By virtue of Eq. (4) the resultant $\mathbf{R}$ must be plotted at the intersection of the two dashed large circles shown in Fig. 11. Shifting the active resultant $\mathbf{R}$ to a safe region is obtained by the addition of vectors $\mathbf{R}+\mathbf{B}$, where $\mathbf{B}$ is the total support force delivered by a cable or rock bolts acting in the direction 270° (W) at 10° inclination below horizontal. This operation is performed along a great circle that connects $\mathbf{R}$ and $\mathbf{B}$ (dotted line in Fig. 11). Thus the total support force required for any factor of safety may be obtained by a simple vector polygon operation, once the angle between the vectors is obtained using stereographic projection techniques.

2-D Versus 3-D Sliding Analysis

The results of the 3-D graphical solution (Fig. 11) are plotted in Fig. 12 together with the results of an "equivalent" 2-D analysis. This comparison can only be made by multiplication of the two-dimensional slice area [Fig. 10(C)] by an equivalent "length," thereby transforming the 2-D slice into an equivalent 3-D prism
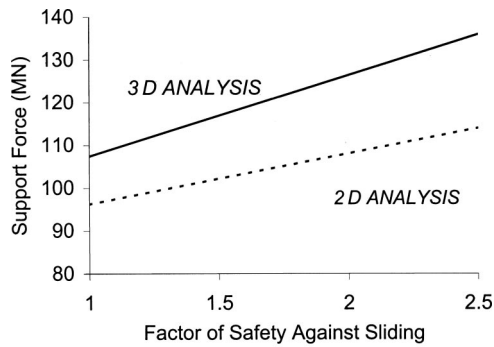
Fig. 12. Two-dimensional (dashed line) versus three-dimensional (solid line) stability analysis for block 1 considering fully saturated joints

with a face-parallel tension crack at the back (Fig. 13). The geometries of the equivalent prism and the true 3-D block are different however: the volume of the real 3-D block as well as the area of the sliding plane which offers shear resistance to sliding are both smaller. The resultant water forces from the two back joints in the true case and from the face-parallel tension crack in the equivalent case are very similar however. Therefore, the real 3-D geometrical configuration of block 1 is less stable than the equivalent 2-D block geometry, in this case by well over 15%.

This result is counterintuitive for most geotechnical practitioners who typically assume that two-dimensional formulation of a slope stability problem represents a more conservative approach. When the stability of rigid blocks subjected to joint water pressures is of concern, it would be more prudent to study the problem in a fully three-dimensional representation.

Pseudo-Static Limit Equilibrium Analysis

By simple extension of the 3-D graphical solution discussed above it is possible to perform a pseudo-static analysis for block 1 sliding either for fully drained or fully saturated conditions. Three-dimensional pseudo-static analysis for blocks, using stereographic projection, was discussed by Goodman (1976, 1989). The pseudo-static inertia force $\mathbf{F_I}$ considered here is horizontal and parallel to the dip-direction of the sliding plane (J_1). Using the block weight, the inertial forces active under peak horizontal ground acceleration of 1.0–0.7 g in 0.1 g increments are calcu-
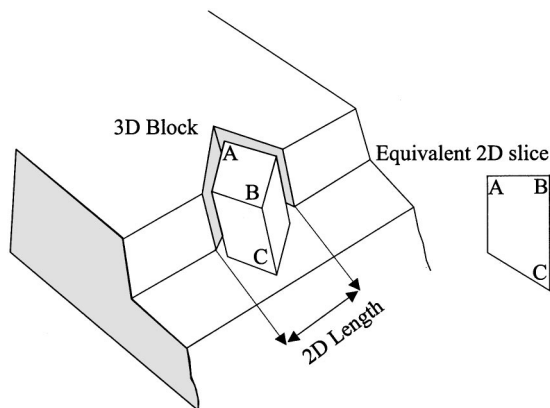

Fig. 13. Prismatic shape of block 1 showing very exaggerated displacement and the assumed "equivalent" 2-D representation
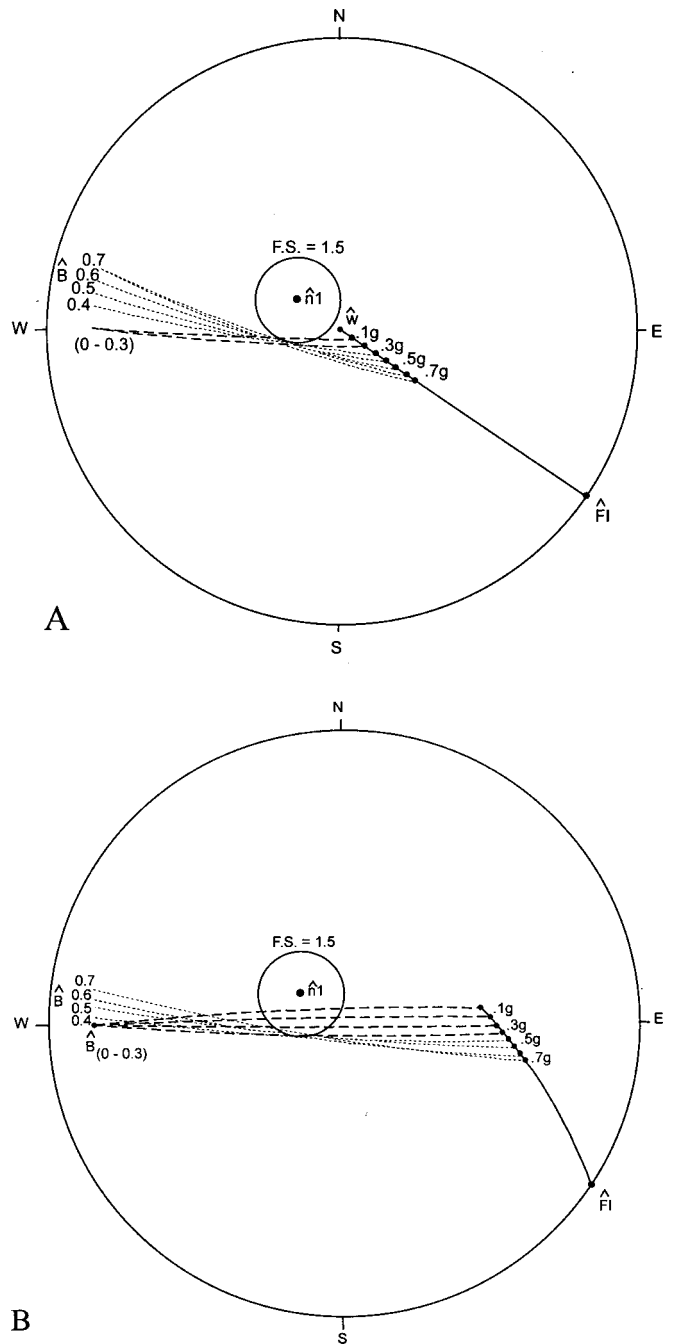

A

B

Fig. 14. Pseudo-static, 3-D analysis for block 1: (A) fully drained and (B) fully saturated conditions

lated, and the new positions are plotted on a large circle that connects the active resultant for static conditions and the inertial force (Fig. 14). The only difference between fully drained and fully saturated analysis is the location of the static resultant. In fully drained analysis the static resultant is the block weight [$\mathbf{W}$ in Fig. 14(A)] whereas in fully saturated analysis the static resultant is $\mathbf{R} = \mathbf{W} + \mathbf{U} + \mathbf{V_2} + \mathbf{V_3}$ [Fig. 14(B)].

Application of support is attained by shifting the new pseudo-static resultant to a friction circle which represents adequate stability. Since the location of the resultant is shifted with an increase in inertial force, the orientation of support force vector $\mathbf{B}$ may have to be changed so that the great circle connecting the pseudo-static resultant and $\mathbf{B}$ will pass through, or at least be tangent to, the friction circle. The results of the 3-D pseudo-static
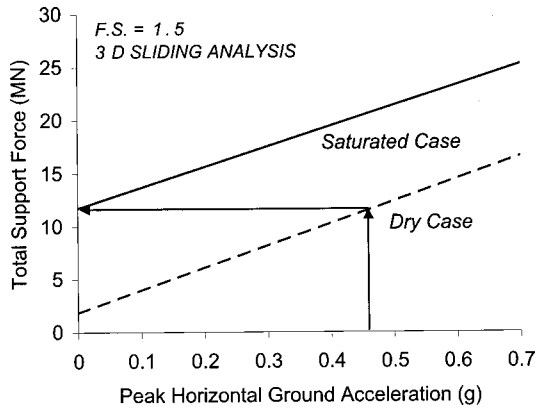
Fig. 15. Results of 3-D pseudo-static analysis for block 1 under fully dry (dashed line) and fully saturated (solid line) conditions; Dotted line: Support installation decision for block 1 in Masada

analyses for block 1 under fully dry and fully saturated conditions are shown in Fig. 15 for a factor of safety of 1.5.

Support Installation

The actual design decision with respect to total support force must address two key issues: (1) the expected site response; and (2) the groundwater regime. The expected site response, in particular the expected peak horizontal ground acceleration (PGA), will determine which level of PGA should be designed, i.e., the x value in Fig. 15. The expected groundwater regime will dictate whether a fully dry or a fully saturated analysis should be performed. Naturally, if saturation is anticipated, effective drains may be installed and support requirements can follow the "dry" curve in Fig. 15.

In the actual stabilization project of the Snake Path cliff, support design for block 1 is shown by the dotted line in Fig. 15. A peak horizontal ground acceleration of 0.45 g was assumed, and drains were installed, therefore a total support force of 12 MN was required in order to insure a factor of safety of 1.5 for pseudo-static loading. The support force applied was designed to sustain full saturation in the joints under static loading conditions.

Note on "Block Slumping" Failure Mode

The tall slender geometry of block 1 makes it susceptible to "block slumping" failure mode, initially proposed by Wittke (1965) and extended to multiple blocks by Kieffer (1998). Because the resultant weight vector trajectory of block 1 acts on the steeply inclined plane (Fig. 16), sliding will commence by mobilizing shear strength along both the steep and the shallow inclined planes simultaneously. Thus, rotation around a center located outside of the block may take place, a failure mode defined as block slumping by Gopodman and Kieffer (2000). It is intuitively clear that once slumping is initiated joint water pressures rapidly dissipate as a joint, with a wide base and sharp edge at the top formed behind the block at the onset of motion.

The forces acting on a block, which undergoes block slumping, are shown in Fig. 16. Assuming the angles of friction on the two sliding planes are equal ($\phi_1 = \phi_2$) three equilibrium equations are necessary for solutions of contact forces N_1 and N_2 and the mobilized angles of friction $\phi_{mobilized}$:
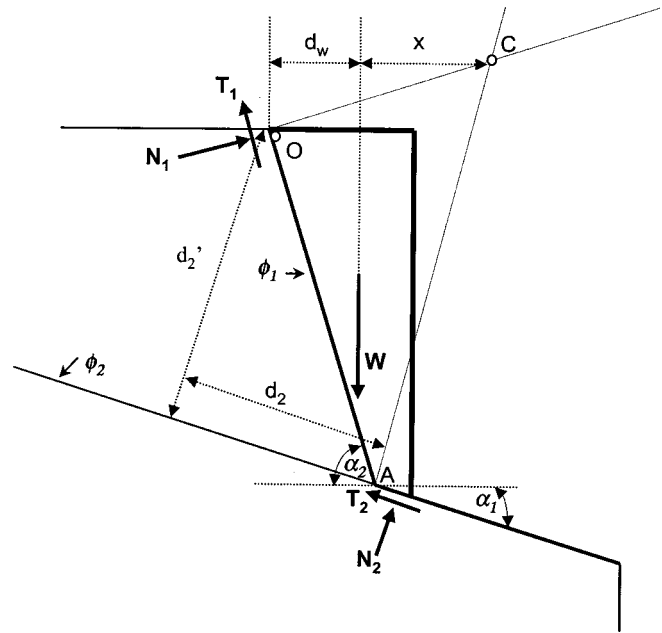

Fig. 16. Free body diagram for block slumping mode (after Kieffer 1998). ϕ_1 and ϕ_2: Angles of friction of the sliding plane and tension crack, respectively; α_1 and α_2: inclination of the sliding plane and tension crack, respectively; point C is the instantaneous center of rotation

$$\Sigma F_v = 0: W = N_1 \cos \alpha_1 + N_1 \tan \phi_1 \sin \alpha_1 + N_2 \cos \alpha_2$$
$$+ N_2 \tan \phi_2 \sin \alpha_2$$
$$\Sigma M_O = 0: W d_w + N_2 \tan \phi_2 d_2' = N_2 d_2 \qquad (5)$$
$$\Sigma M_C = 0: W x = N_2 \tan \phi_2 AC + N_1 \tan \phi_1 OC$$

where α_1 and α_2=inclinations of the sliding plane and of the tension crack, respectively. Simultaneous solution of the three equations for the geometry of block 1 [Fig. 10(C)] yields a mobilized angle of friction value of $\phi_{mobilized} = 22°$. This failure mode is therefore slightly less stable than the sliding mode discussed above, which requires a friction angle of 20° for stability.
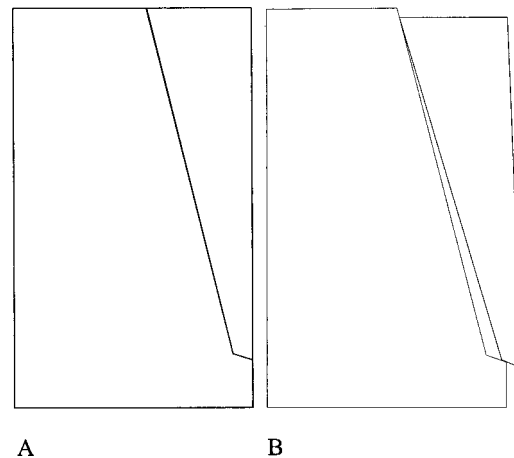

Fig. 17. Simulation of block slumping failure mode for the geometry of block 1 using DDA (time step size 0.01 s, stiffness of contact springs 5×10^9 N/m: (A) ϕ on both joints of 24° and (B) ϕ on both joints of 21° at $t = 1$ s

We can therefore conclude that with a friction angle greater than 22° the block is safe from slumping. In order to check the validity of this analysis the dynamic motion of block 1 was modeled using DDA (Shi 1993) with the same geometry as that in Fig. 10(C). DDA simulation with $\phi_1 = \phi_2 = 24°$ did not result in any block displacement [Fig. 17(A)] but with $\phi_1 = \phi_2 = 21°$ block slumping with a loss of contact at the base after 1.5 s was predicted [Fig. 17(B)].

The support force for block 1 using 2-D dry, pseudo-static analyses for block sliding and block slumping yields similar results (within 5%), with the slumping mode being slightly more demanding (details of the support analysis will be the subject of a separate paper). The actual support scheme for block 1 in this project followed the design chart shown in Fig. 15 taking full advantage of the more accurate 3-D analysis which roughly requires 15% more support capacity than the 2-D sliding mode, when everything else is equal (loading and water conditions). Nevertheless, the support requirements for slumping and sliding may vary, depending upon the particular block geometry. Therefore, both modes must be checked before a support decision is made.

Summary and Conclusions

Two issues that pertain to rock slope stability were studied in this paper: (1) time dependent displacement behavior of removable keyblocks; and (2) stability and mode analysis of removable keyblocks.

Using a comprehensive monitoring program insight was gained into the nature of removable keyblock displacement over time. It was shown that climatic effects may lead to substantial block displacements, up to 0.8 mm over a period of several months, some of which may be recovered at the end of a season. The long-term effect of such very long period cyclic deformation on the shear strength of joint interfaces remains to be studied; cyclic deformation over a long period certainly leads to shear strength degradation and cohesive bond deterioration over time.

In stability analysis of prismatic blocks under saturated conditions it is strongly advisable to adopt a fully three-dimensional approach. It was shown in this paper that for the geometry of the keyblock studied, an equivalent two-dimensional analysis is not conservative with respect to the support force required by as much as 15%.

It is also strongly recommended that one conduct a fully three-dimensional analysis for support design under pseudo-static loading. Such an approach will allow the engineer to optimize the direction of the support installed and to better estimate the magnitude of the support necessary.

Tall slender blocks which are separated from the rock mass by a steeply inclined joint at the back, and which rest over a moderately inclined discontinuity at the base (typically a bedding plane), may be susceptible to block slumping failure mode. It is important to detect the correct failure mode accurately because the block slumping mode is less stable than the single plane sliding mode, if the same base plane is considered and everything else is equal. Therefore, failure to assess the failure mode correctly could lead to unconservative evaluation of the stability.

There is also an economic advantage in accurate failure mode assessment: if block slumping is the critical failure mode it could be argued that drained conditions will always prevail in the field without having to install artificial drainage since sliding would be followed by significant enlargement of the steep joint aperture at the back of the block.

References

Abrahamsom, N. A., and Sheldock, K. M. (1997). "Overview." *Seismol. Res. Lett.,* 68(1), 9–23.

Abrahamson, N. A., and Silva, W. J. (1977). "Empirical response spectral attenuation relations for shallow crustal earthquakes." *Seismol. Res. Lett.,* 68(1), 94–127.

Eyal, M., Eyal, Y., Bartov, Y., and Steinitz, G. (1981). "The tectonic development of the western margin of the Gulf of Elat (Aqaba) rift." *Tectonophysics,* 80, 39–66.

Feund, R. (1965). "A model of the structural development of Israel and the adjacent areas since Upper Cretaceous times." *Geol. Mag.,* 102, 189–205.

Garfunkel, Z. (1981). "Internal structure of the Dead Sea leaky transform (rift) in relation to plate kinematics." *Tectonophysics,* 80, 81–108.

Garunfkel, Z., Zak, I., and Freund, R. (1981). "Active faulting in the Dead Sea rift." *Tectonophysics,* 80, 1–26.

Goodman R. E. (1976). *Methods of geological engineering in discontinuous rocks,* West Publishing, St. Paul, Minn.

Goodman R. E. (1989). *Introduction to rock mechanics,* 2nd Ed., Wiley, New York.

Goodman, R. E., and Kiefer, D. S. (2000). "Behavior of rock in slopes." *J. Geotech. Geoenviron. Eng.,* 126(8), 675–684.

Goodman, R. E., and Seed, H. B. (1966). "Earthquake induced displacements in sands and embankments." *J. Soil Mech. Found. Div.,* 92(2), 125–146.

Hatzor, Y. H., and Goodman, R. E. (1997). "Three dimensional back analysis of saturated rock slopes in discontinuous rock—A case study." *Geotechnique,* 47(4), 817–839.

Kieffer, D. S. (1998). "Rock slumping—A compound failure mode of jointed hard rock slopes." PhD dissertation, Dept. of Civil and Environmental Engineering, U.C. Berkeley, Berkeley, Calif.

Londe, P. F., Vigier, G., and Vormeringer, R. (1970). "Stability of rock slopes—Graphical methods." *J. Soil Mech. Found. Div.,* 96(4), 1411–1434.

Mironer, A. (1979). *Engineering fluid mechanics,* McGraw-Hill, New York.

Newmark, N. M. (1965). "Effects of earthquakes on dams embankments." *Geotechnique,* 15, 139–160.

Shi, G.-H. (1993). *Block system modeling by discontinuous deformation analysis,* Computational Mechanics, Southampton, U.K., 209.

Talobre, J. A. (1967). *La mecanique de roches et ses applications,* 2nd Ed., Dunod, Paris.

Wittke, W. (1965). "Methods to analyze the stability of rock slopes with and without additional loading." *Rock Mech. Eng. Geol., Supp. II* (in German).

Zaslavski, Y., Shapira, A., and Leonoy, J. (1998). "Topography effects and seismic hazard assessment at Mt. Massada (Dead Sea)." *Rep. No. 522/62/98,* The Geophysical Institute of Israel.

ERRATA

Errata for "Keyblock Stability in Seismically Active Rock Slopes—Snake Path Cliff, Masada" by Yossef H. Hatzor

On p. 708, in Fig. 12 where a comparison between a three-dimensional and an equivalent two-dimensional stability analysis for block sliding with full water head inside the boundary joints is shown, the y-axis values representing support load in MN are mistakenly high by one order of magnitude. The support force values shown in Fig. 15 are correct. A correct version of Fig. 12 is shown below:
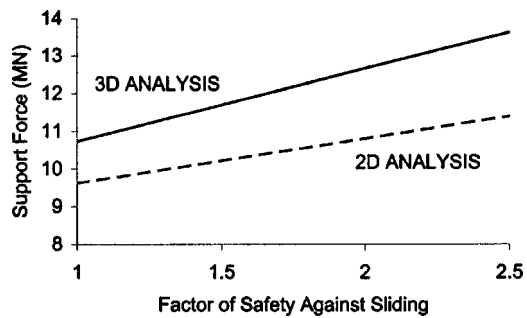

Fig. 12. Two-dimensional (dashed line) versus three-dimensional (solid line) stability analysis for Block 1 considering fully saturated joints